PAPER • OPEN ACCESS

Diamond micro-milling of lithium niobate for sensing applications

View the article online for updates and enhancements.

Diamond micro-milling of lithium niobate for sensing applications

Dehong Huo[1], Zi Jie Choong[1], Yilun Shi[1], John Hedley[1] and Yan Zhao[2]

[1] School of Mechanical and Systems Engineering, Newcastle University,
Newcastle Upon Tyne NE1 7RU, UK
[2] School of Mechanical Engineering, Yanshan University, Qinhuangdao 066004, People's Republic of China

E-mail: dehong.huo@newcastle.ac.uk (D Huo)

CrossMark

Abstract

Lithium niobate (LiNbO$_3$) is a crystalline material which is widely applied in surface acoustic wave, microelectromechanical systems (MEMS), and optical devices, owing to its superior physical, optical, and electronic properties. Due to its low toughness and chemical inactivity, LiNbO$_3$ is considered to be a hard-to-machine material and has been traditionally left as as an inert substrate upon which other micro structures are deposited. However, in order to make use of its superior material properties and increase efficiency, the fabrication of microstructures directly on LiNbO$_3$ is in high demand. This paper presents an experimental investigation on the micro machinability of LiNbO$_3$ via micro milling with the aim of obtaining optimal process parameters. Machining of micro slots was performed on *Z*-cut LiNbO$_3$ wafers using single crystal diamond tools. Surface and edge quality, cutting forces, and the crystallographic effect were examined and characterized. Ductile mode machining of LiNbO$_3$ was found to be feasible at a low feed rate and small depth of cut. A strong crystallographic effect on the machined surface quality was also observed. Finally, some LiNbO$_3$ micro components applicable to sensing applications were fabricated.

Keywords: micro milling, lithium niobate, ductile mode cutting, diamond tool, crystallographic effect, edge chipping, sensors

(Some figures may appear in colour only in the online journal)

1. Introduction

Single crystal lithium niobate (LiNbO$_3$) has attracted attention from many researchers for its wide range of applications in surface acoustic wave, radio-frequency telecommunications, and optical devices owing to its superior physical, optical, and electronic properties (Wong 2002). In recent years, LiNbO$_3$ has shown potential in microelectromechanical systems (MEMS) and biosensor applications (Okayama 2003) due to the fact that it is superior to silicon-based materials in terms of mechanical and electrical performance. There is an increasing need to fabricate microstructures, such as microfluidic channels and diaphragms, on LiNbO$_3$ directly. However, due to its low toughness, high anisotropy, and chemical inactivity, LiNbO$_3$ is considered to be a hard-to-machine material and has been traditionally left as an inert substrate upon which other micro structures are deposited (Tseng 2006, Johansson, 2012, Sridhar 2012).

Interestingly, although mechanical grinding has been used to dice LiNbO$_3$, very little research has been reported on employing mechanical micro cutting approaches in shaping LiNbO$_3$ micro structures. Micro milling, an emerging micro manufacturing process, has been successfully applied to the fabrication of 3D complex-shaped micro components with excellent dimensional accuracy and surface finish over a variety of engineering materials (Cheng 2013). Recently it has been successfully applied in machining brittle materials and crystals, such as graphite (Huo 2014), single crystal silicon (Rusnaldy 2007, 2008, Arif 2012, Choong 2015, Huo 2015), ceramics (Cho 2007) and glass (Foy 2009, Arif 2011). Micro

milling is therefore expected to have the potential to cost effectively fabricate complex-shaped $LiNbO_3$ micro components with feature sizes at the order of several tens to several hundred microns. Success of micro milling $LiNbO_3$ will open new industrial avenues in the fabrication of $LiNbO_3$ micro products and fill the gap of fabrication of micro/meso scale components for prototype or small batch production.

In this paper, an experimental investigation is presented on the micro machinability of $LiNbO_3$ via micro milling with the aim to obtain optimal process parameters. Machining of micro slots was performed on single crystal $LiNbO_3$ wafers using single crystal diamond tools. Surface and edge quality, cutting forces, and crystallographic effects were examined and characterized. Based on results obtained from the machinability study, some $LiNbO_3$ micro components applicable to sensing applications were fabricated.

2. Current fabrication techniques

Device shaping on $LiNbO_3$ has been continuously reported for being difficult to machine. This is because $LiNbO_3$ is highly anisotropic, brittle, inert to most etchants and transparent to most laser wavelengths (Lee 1995). Manufacturing processes, namely wet or dry etching, laser micromachining and mechanical micromachining methods had been researched for fabricating profiles such as micro-channels on $LiNbO_3$. With the increasing need for a precise etching technique, research to enhance the chemical reactivity for wet etching was focused through the development of ion implantation approaches. These processes include focused ion beam (FIB) milling, reactive ion beam etching and deep reactive ion etching (DRIE) (Wong 2002).

Sridhar *et al* performed FIB milling to fabricate micro-channels in $LiNbO_3$ (Sridhar *et al* 2012). *Y*- and *Z*-cut samples were used and micro-channels 10 μm long with widths of 1 and 0.5 μm were fabricated at three different ion currents. Results showed that the material removal rate decreases with respect to the aspect ratio of the final milled structure when the ion dose increases. Low aspect ratio structures can therefore be milled directly, however material re-deposition is needed if deeper structures with a high aspect ratio are required. With the involvement of argon, reactive ion beam etching allows a higher material removal rate when compared to FIB milling (Chapman 1984). DRIE was also studied and shown to achieve better etching results compared to FIB milling and reactive ion beam etching (Darbyshire 1986). Using lower pressure plasma and placing the sample in a DC bias, the sample is attacked by both chemical reactions with plasma ions and also directional ions which bombard the substrate when accelerated across the cathode (Winnall 2000). This allows the etching rate to increase due to the generation of higher ion energies.

Laser micromachining was also researched for direct fabrication on $LiNbO_3$. Greuters *et al* performed laser micromachining using 355 nm Nd:YVO$_4$ and 193 and 248 nm excimer lasers (Greuters and Rizvi 2003). Good quality results were obtained from the 355 nm and both excimer lasers. In addition, the crystallographic orientation effect was deemed to be insensitive when compared to those of DRIE (Winnall and Winderbaum 2000). Malshe *et al* performed laser micromachining using a femtosecond laser. A distinct advantage of a femtosecond laser compared to those of micro or nanoseconds is the redeposition due to ultrashort lasing pulses (Malshe *et al* 2004). A thin layer of amorphous region was identified on the surface after laser micromachining. Lin *et al* also performed laser micromachining with a femtosecond laser to create a free standing microresonator (Lin *et al* 2015). The entire machining process involved femtosecond laser micromachining with FIB milling and high quality microresonators were produced.

Although wet etching, ion implantation, FIB milling and laser micromachining have been studied for device shaping of $LiNbO_3$, these processes suffer relatively low material removal rate and are only economical for high volume production. Alternatively, mechanical micromachining also shows potential in $LiNbO_3$ manufacturing. Okuda *et al* conducted planer-type cutting using diamond tools to fabricate micro grooves with varying depth up to 50 μm and confirmed that the edge quality of the groove affects the propagation mode of the surface acoustic wave (Okuda 2014). Takigawa *et al* employed ultra-precision cutting in the fabrication of $LiNbO_3$ ridged waveguides (Takigawa 2014). A smooth finish of approximately 4.5 nm was achieved on the machined sidewalls and thus reduces scattering losses of guided light. Currently, investigations on micro milling of $LiNbO_3$ are very limited, notably, Al-Shibaany *et al* performed hole drilling experiments using end milling and characterised the sub-surface strains using Raman spectroscopy (Al-Shibaany *et al* 2014); Shizuka *et al* (2010) conducted micro milling experiments using tungsten carbide tools and discussed the crystallographic effect. The feasibility of forming micro grooves was proven and the ductile mode was observed to be at a 5 μm depth of cut or less (Shizuka *et al* 2010).

3. Experiments

3.1. Experimental setup

Experiments for this work were carried out on an ultra-precision desktop micro machining centre (Nanowave MTS5R). The machine is equipped with a high speed aerostatic bearing spindle (Air Bearings Ltd) offering a speed of 18 000 rpm–180 000 rpm. The high speed spindle allows a high cutting velocity even when small diameter cutters are used. The *XYZ* sliders provide a precision of 0.1 μm. This experimental set-up ensures that both the spindle errors such as vibration and run-out, and slideway inaccuracy were minimised. Therefore spindle and slideway errors on surface quality will not be explicitly taken into account in the analysis. A multi-component piezoelectric cutting force dynamometer (Kistler MiniDyn type 9256C2) was mounted on the top of a *Z* slide to monitor the cutting force during machining and also assist the cutting tool set-up. The experimental set-up is illustrated in figure 1.
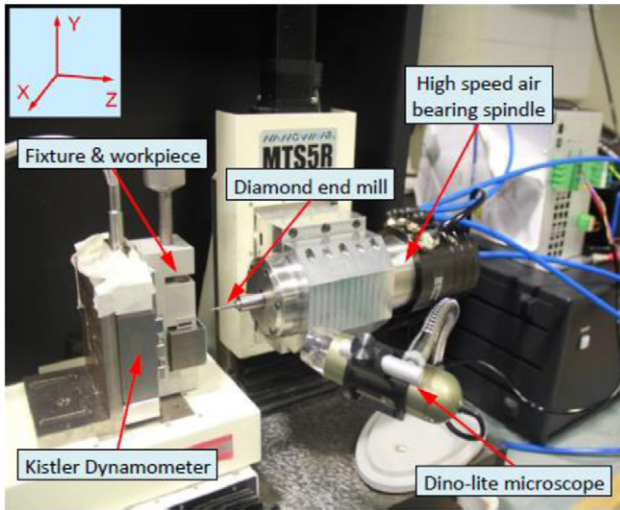
Figure 1. Experimental set-up and working coordinates.

Polished *Z*-cut LiNbO$_3$ samples (dimension 10 mm × 10 mm × 0.5 mm) were used in this research. The samples were adhesively bonded onto a ground stainless steel fixture and removed using acetone after machining. Single flute single crystal diamond micro milling tools (Contour Fine Tooling) with a nominal diameter of 0.3 mm were used in the experiments. A uniform tool shank diameter of 3 mm is used for all micro tools to fit a 3 mm ultra-precision spindle collet. Figure 2 shows the micro end mills used in the experiments.

3.2. Experimental procedure

Prior to the machining experiments, the levelness of the square LiNbO$_3$ wafer surface to the cutting tool axis was carefully adjusted using a 1 μm resolution dial gauge. A levelness deviation of less than 5 μm was obtained over the 10 mm × 10 mm machining area. To eliminate the effect of levelness deviation on the depth of cut, the NC program (Z feed) was also adjusted to compensate for this geometric error thanks to the 0.1 μm feed precision of the machine tool. Zero position of the cutting tool relative to the LiNbO$_3$ wafer surface was set with the assistance of a machine vision system (Dino-lite microscope) and initial contact test using the Kistler dynamometer at a very slow feed rate. This procedure allows one to set up the depth of cut at a micron level.

Full immersion slot milling was performed in this experiment. No coolant was used to avoid contamination, and compressed air was supplied throughout the machining experiments to reduce the possibility of chip jam induced micro cracks. Two sets of machining experiments were carried out to investigate the influence of the cutting parameters and crystallographic effect on the surface quality, respectively.

In the first set of experiments, 5 mm long and 0.3 mm wide micro slots were milled along a fixed [1 0 $\bar{1}$ 0] direction. The three controlled quantitative factors used in the experiments are cutting speed (m min^{-1}), feed rate (μm/tooth) and axial depth of cut (μm). Due to the presence of only three controlled
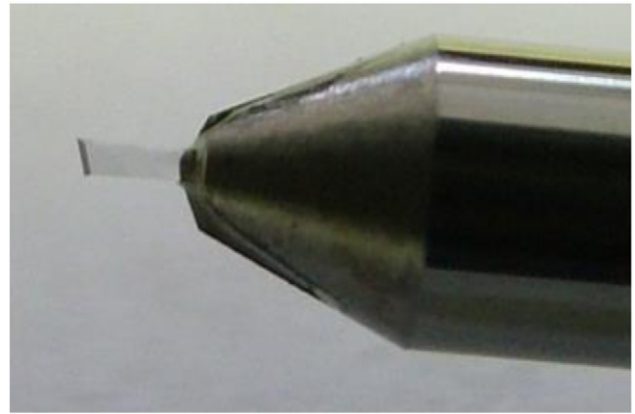

Figure 2. Single crystal diamond micro milling tool used in the experiments.

Table 1. Cutting parameters used in the first set of experiments.

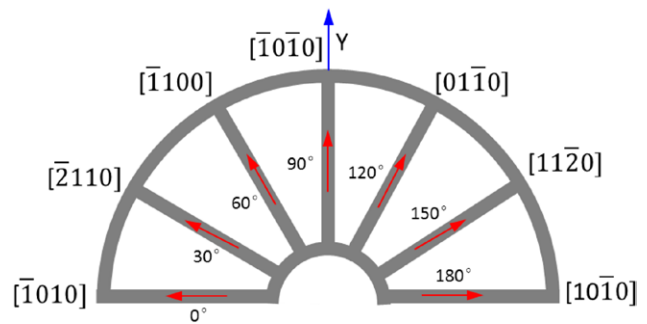| Cutting parameters	Values
Feed per tooth (μm/tooth)	0.1, 0.3, 0.6, 1.0
Axial depth of cut (μm)	1, 5, 10
Spindle speed (rpm)	20 000, 50 000

Figure 3. Feed directions in the second set of experiments.

factors, full factorial experimental designs were implemented to capture the entire main effects and their interactions. Two levels of cutting speed, three levels of depth of cut, and four levels of feed rate were selected. The cutting parameters in this 2 × 3 × 4 mixed level full factorial design is presented in table 1. Each set of cutting parameters was repeated to reduce machining errors and separate the influence due to interactions from the measurement noise. A total of 48 slots were machined for each cutter. In order to reduce the influence of tool wear on the surface quality and edge chipping, a brand new micro tool was used for the experiments.

In the second set of experiments, 5 mm long and 0.3 mm wide micro slots were milled along various crystallographic directions for studying the crystallographic orientation effect. The cutting parameters were fixed using optimal cutting speed and feed rate obtained from the first set of experiments. Figure 3 shows the schematic feed direction in the second experiments.

After the machining experiments, the machined surface was cleaned in acetone by an ultrasonic bath. The average surface
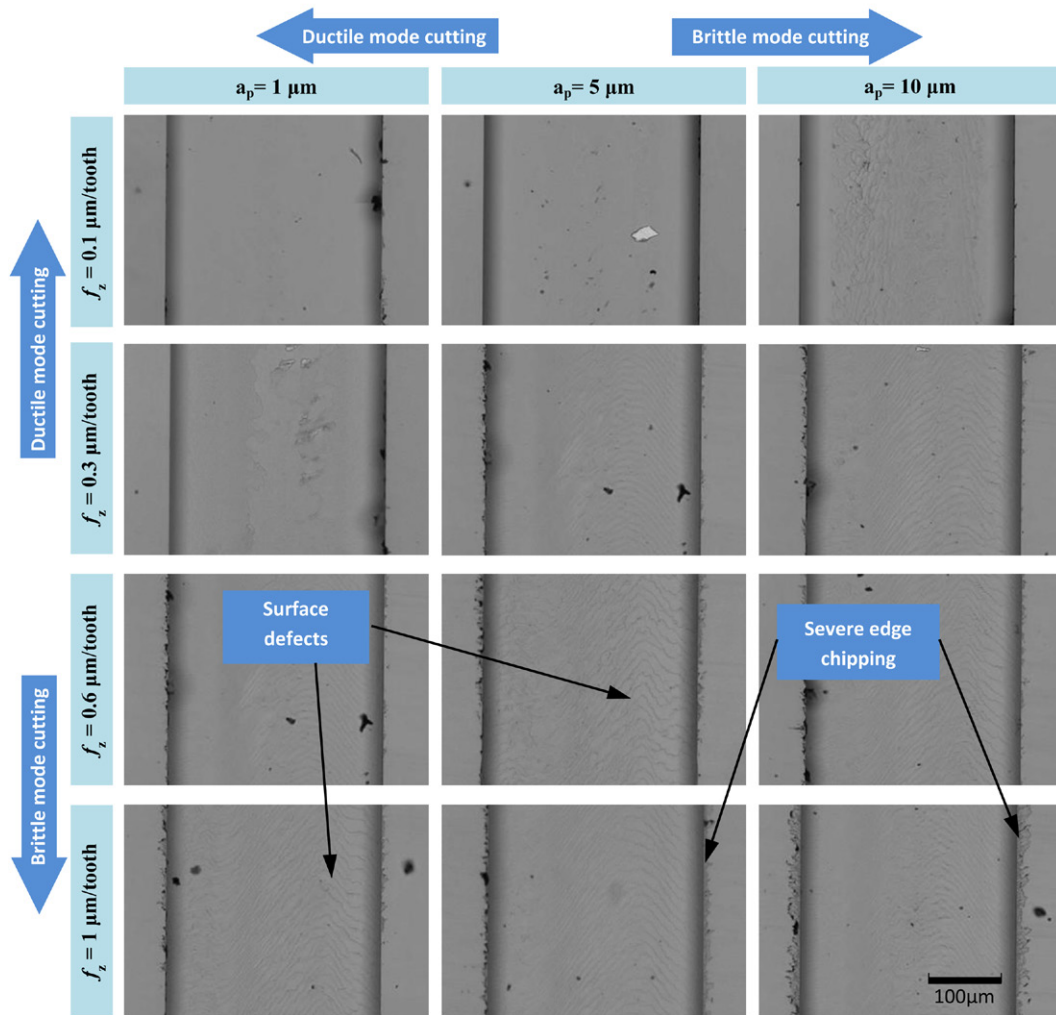
Figure 4. Machined surface topography at different feed rate and depth of cut (cutting speed: 31.4 m min^{-1}).

roughness of the bottom surface for each micro-milled slots was then measured using a white light interferometer (Zygo NewView 5020). To reduce the measurement uncertainty, four measurements on different areas were conducted for each slot and an average value of surface roughness (Ra) is used for analysis. The surface morphology and burr formation were analysed on the basis of SEM micrographs. Cutting forces and specific cutting energy were calculated and analysed.

4. Results and discussion

Both qualitative and quantitative analyses were carried out to characterise surface and edge quality of micro-milled slots. Qualitative analysis includes burrs formation, cutting mode observation, and surface topography, and quantitative analysis includes surface roughness and specific cutting energy analysis.

4.1. Surface topography and edge chipping

Surface characterisation of the machined slots was performed using an SEM and a 3D surface profilometer. Figure 4 shows the SEM micrographs of the micro machined slots. Surface

defects were found on the micro machined surface and edge chipping was observed in most of the slots. The results show that the feed rate and axial depth of cut have significant influence on the surface generation. Higher cutting speed is also found to promote better surface quality. Slow feed rate and small axial depth of cut produce fewer surfaces defects and hence promote ductile mode machining. Figure 5 shows surface measurement results on typical ductile and brittle mode machined surfaces. On the ductile mode machined surface, regular tool marks and less surface defects were observed. Surface roughness measurements indicate that a very smooth surface with surface roughness $Ra = 10$ nm can be achieved at $f_z = 0.1$ μm/tooth and $a_p = 1$ μm. In contrast, on the brittle mode machined surface, regular tool marks are absent and instead irregular streaks were observed, and surface roughness, $Ra = 50$–150 nm, was measured.

As already demonstrated in previous single point diamond turning (SPDT) experiments, an enabling factor for ductile mode machining of brittle materials is the use of very small uncut chip thickness and depth of cut. It is believed that there is a critical uncut chip thickness, below which the energy required to cause fracture is higher than that required for plastic deformation. Therefore, plastic deformation becomes
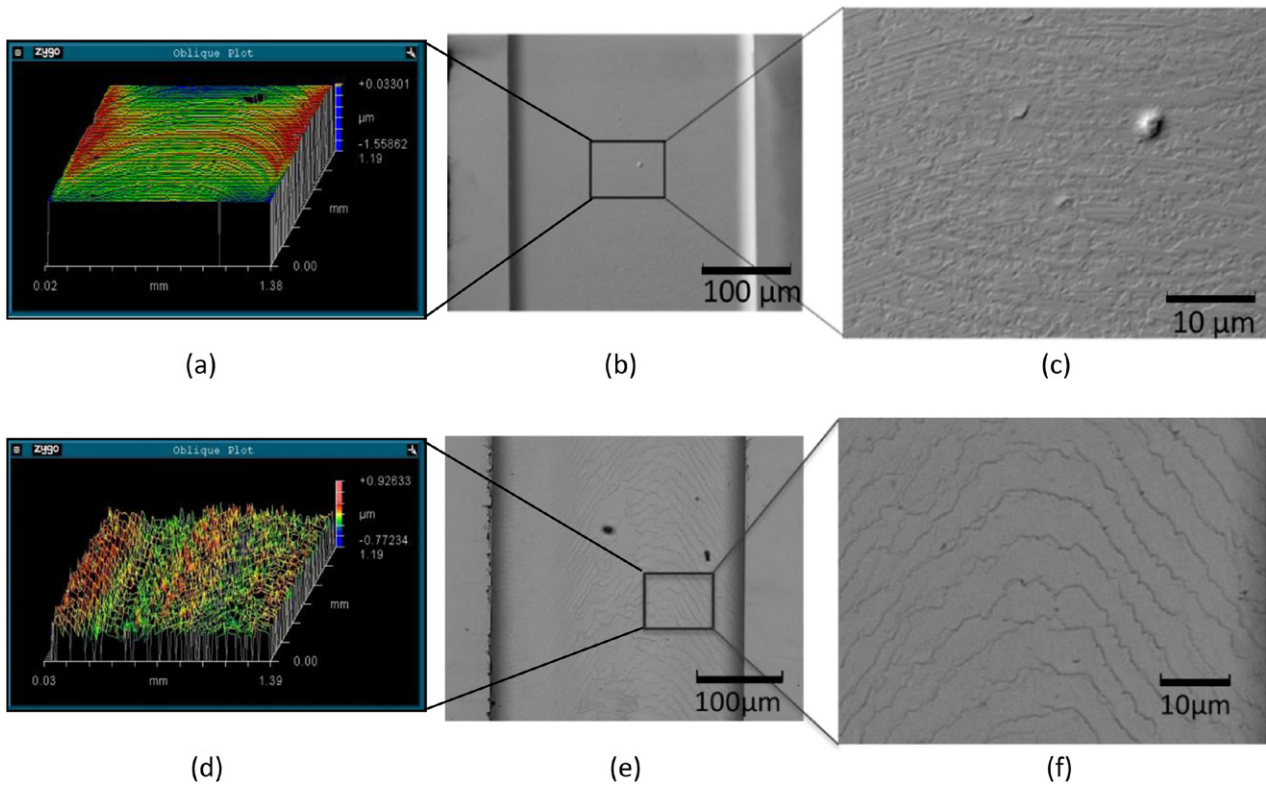
Figure 5. Examples of ductile and brittle mode machined surface: (a)–(c) ductile mode machined surface; (d)–(f) brittle mode machined surface; (a) and (d) Zygo surface profilometer surface roughness measurement.

the primary mechanism of material removal instead of brittle fracture (Li *et al* 2010, Yan *et al* 2009). When materials undergo ductile shear plastic deformation, lesser surface and subsurface defects are generated and hence better surface roughness can be achieved.

Edge chipping is a type of surface/subsurface defect normally induced in the machining of brittle materials. Machining induced edge chipping affects the geometric accuracy of the finished parts and causes potential functional failure due to the micro cracks left on the finished part (Ng 1996, Gong 2013). Good edge quality in some $LiNbO_3$ applications is believed to be more desirable than surface roughness. In the micro milling of micro devices, the size of edge chipping defects can be comparable to its feature size, therefore control and suppression of edge chipping formation in micro milling becomes a pressing challenge. The SEM micrographs in figure 4 show a similar trend as surface topography, i.e. lower feed rate and axial depth of cut would produce less edge chipping defects due to ductile mode machining. In a full immersion milling operation, both up and down milling sides of the slot are generated. In the up milling side, the cutting direction is opposite to the workpiece feed direction and the surface is generated at the beginning of the cut, whilst the cutting direction is the same as the feed direction in the down milling side and the surface is generated when the cutting edge exits the workpiece. Therefore, up and down milling have different characteristics in edge chipping formation. Within the machining conditions in this experiment, edge chipping defects were predominantly observed in the down milling side of the slot, and lesser or no edge chipping in the up milling side were formed as shown
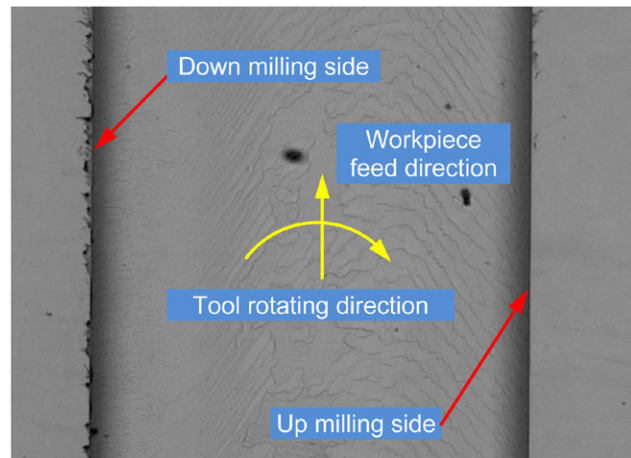
Figure 6. SEM micrographs of micro milled slots showing interior edge chipping.

in figure 6. Brittle materials like $LiNbO_3$ are more sensitive to impact at workpiece entry. In the case of up milling, the nominal instantaneous uncut chip thickness starts from minimum chip thickness (a few tens of nanometers in this case) and increases gradually, therefore lesser edge chipping defects are formed. This conclusion is in agreement with the micro milling of other brittle materials (Huo 2015).

4.2. Specific cutting energy

The cutting forces were collected by the dynamometer during the machining process to calculate the specific cutting energy.
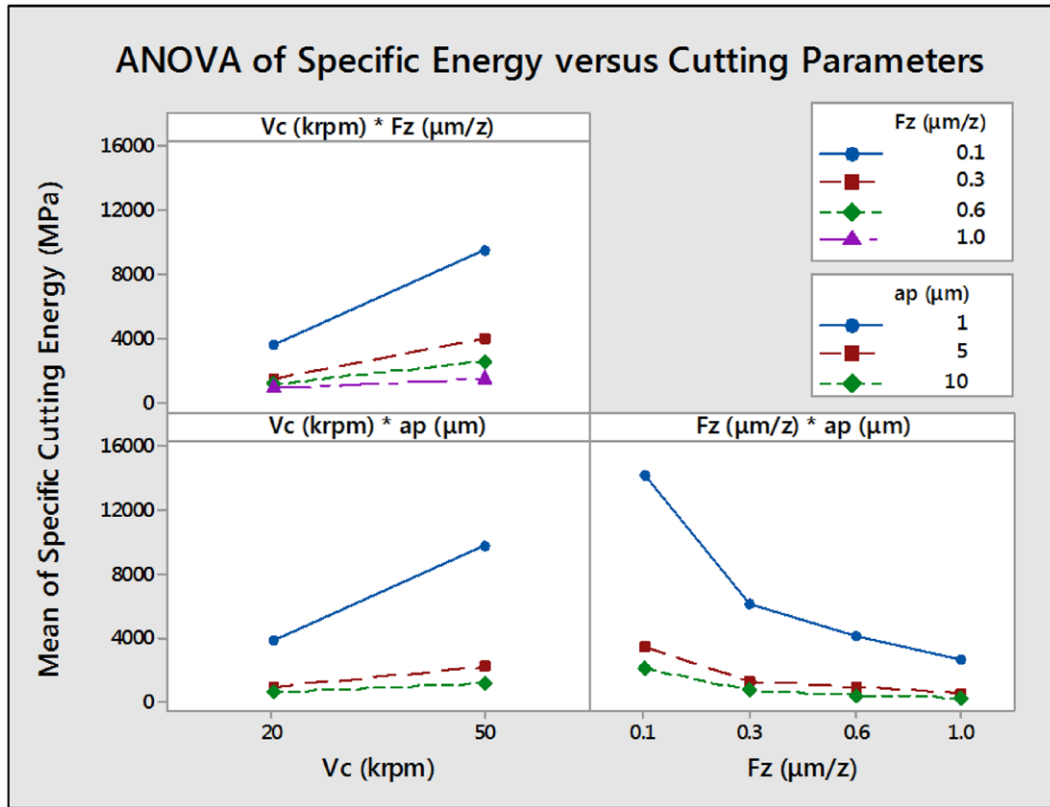
Figure 7. Factorial plots of specific cutting energy versus cutting parameters.

Firstly, raw force data was used to obtain the principle cutting forces and thrust forces, via equation (1):

$$\begin{pmatrix} \mathrm{d}Fx(\theta) \\ \mathrm{d}Fy(\theta) \end{pmatrix} = \begin{pmatrix} -\cos\theta & -\sin\theta \\ \sin\theta & -\cos\theta \end{pmatrix} \begin{pmatrix} \mathrm{d}Ft(\theta) \\ \mathrm{d}Fr(\theta) \end{pmatrix} \quad (1)$$

where Fx and Fy represent the measured cutting forces along the feed and cross feed directions respectively, while Ft and Fr represent the thrust and cutting forces, and θ is the rotation angle of the cutting. Then specific cutting energy, or specific cutting force (unit: MPa), Uc, is defined as follows:

$$Uc = \frac{V_c}{V_{\mathrm{rem}}} \times \int_0^{T_c} \sqrt{Ft^2 + Fr^2}\,\mathrm{d}t \quad (2)$$

where V_c and V_{rem} stand for the cutting speed and material removal volume, with T_c as the cutting time.

It has been proven that the specific cutting energy required by plastic deformation of the material is higher than that required by brittle rupture (Wang 2008). Thus, it would also be an indication of brittle-ductile transition occurring should a drop of the specific cutting force be observed.

Analysis of variance (ANOVA) performed on the cutting force data (figure 7) indicates that, within the experimental machining conditions, a lower depth of cut or a slower feed rate results in higher specific cutting energy, hence indicating that a ductile mode cutting has taken place. As shown in figure 7, when depth of cut of 1 μm is used, a feed rate decrease from a 1 μm/tooth to 0.1 μm/tooth would result in an increase of specific cutting energy from 2000 MPa to 14 000 MPa and also a steep increase from the feed rate of a 0.3 μm/tooth can be observed suggesting that a 0.3 μm/tooth

could be the brittle-ductile transition threshold. When a 0.1 μm/tooth is used, a depth of cut decrease from 10 μm to 1 μm would result in an increase of specific cutting energy from 1800 MPa to 14 000 MPa. It can also be seen from figure 7 that a higher cutting speed results in higher specific cutting energy. Therefore, higher specific cutting energy, which has been believed to be a sign of ductile machining, is obtained with higher cutting speed, along with a lower feed rate and cutting depth. This conclusion is consistent with results from the surface topography analysis, which in turn proves that specific cutting energy can be used as an effective indicator of the cutting mode for brittle materials. Attempts were also made to look into the ratio of thrust force and principle cutting force, however, the theory stating that under a critical uncut chip thickness, the thrust force stays larger than the principle cutting force (Davim 2008) was not supported by the results from the micro milling of LiNbO$_3$ in this experiment.

4.3. Crystallographic effect

In order to study the effect of crystallographic orientation of the material on the surface quality, slots along different crystallographic orientations were machined using single crystal diamond tools using the same cutting parameters, as described in section 3.2. The machining parameters used in the second set of experiments were: spindle speed, $n = 50\,000$ rpm; feedrate, $f_z = 0.1$ μm/tooth; depth of cut, $a_p = 5$ μm. Although almost crack-free surfaces were found to be achieved in the first set of experiments (feedrate, $f_z = 0.1$ μm/tooth and a
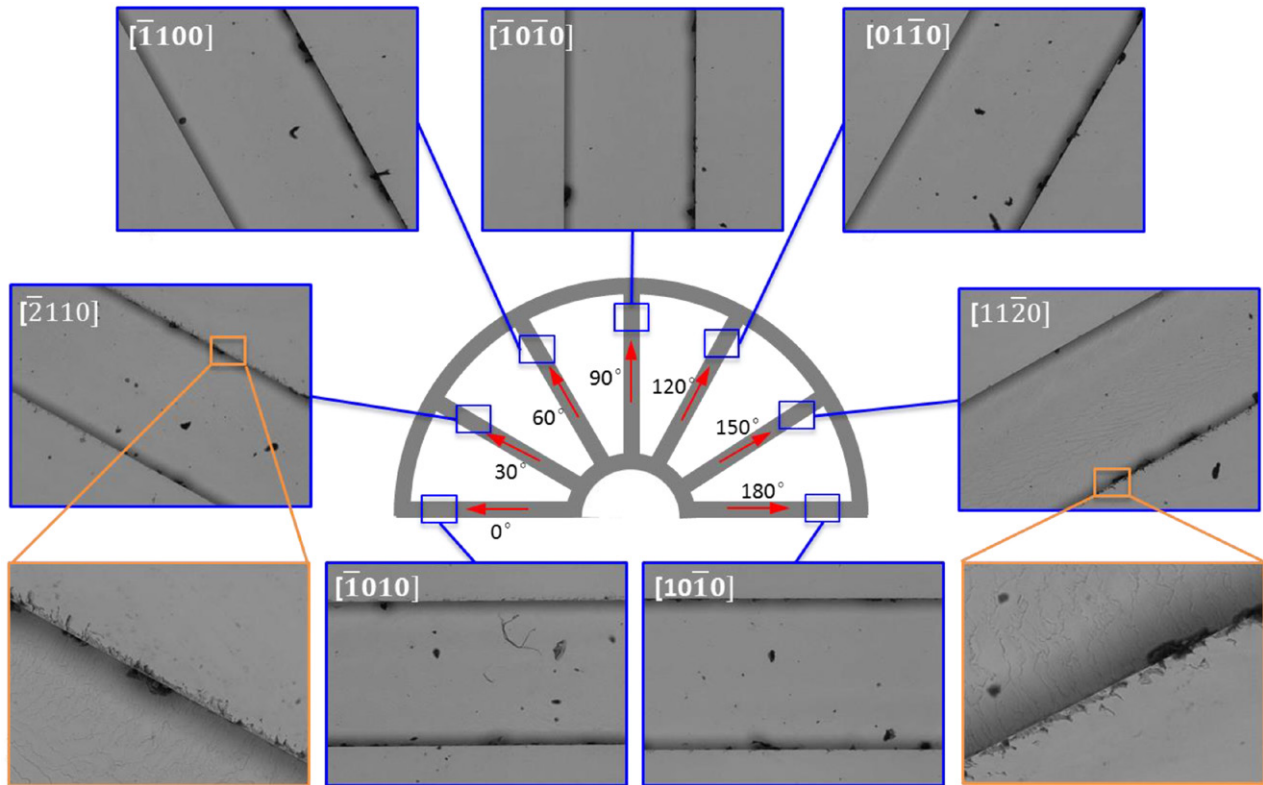
Figure 8. Crystallographic effect on the surface and edge quality.

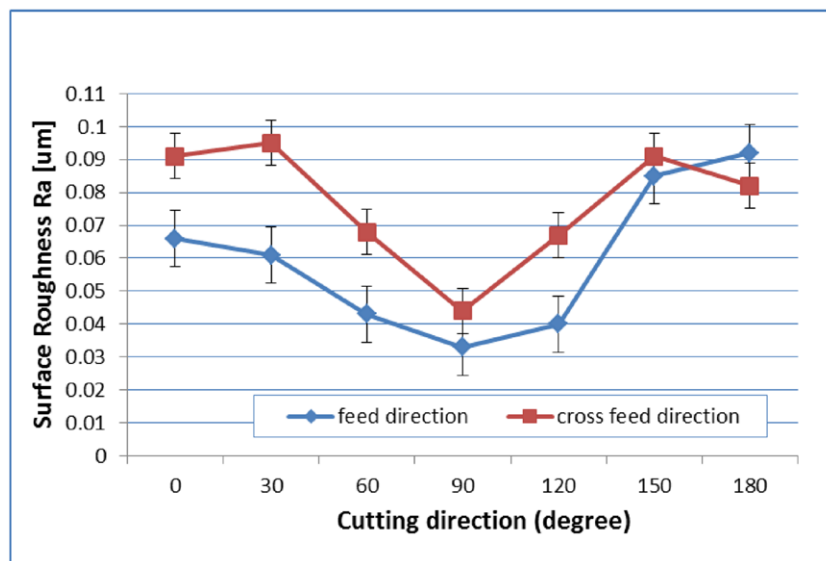**Figure 9.** Crystallographic effect on the surface roughness.

depth of cut, $a_p = 1$ μm), a slightly deeper depth of cut was used to show the distinct differences along different crystallographic orientations.

Cleavage planes of LiNbO$_3$ naturally run along the family planes of $\{01\bar{1}2\}$ (Boyd 1964, Weis 1985). Since LiNbO$_3$ has a hexagonal crystalline configuration, it exhibits a threefold symmetry in which its cleavage planes repeat itself at every 120°. Due to the anisotropy property of the material, a strong crystallographic orientation effect was observed. As

shown in figure 8, edge chipping defects were observed in the slots machined along the cleaving directions of $[\bar{2}110]$ (30°) and $[11\bar{2}0]$ (150°). This is due to the cleaving directions having lower surface energies and hence having less resistance to edge chipping generation during contact with the cutting tool. Good edge quality without obvious chipping defects were achieved by the slots machined other directions. Evident differences on the edge quality were shown between the up-milling and down-milling sides on the machined slots.
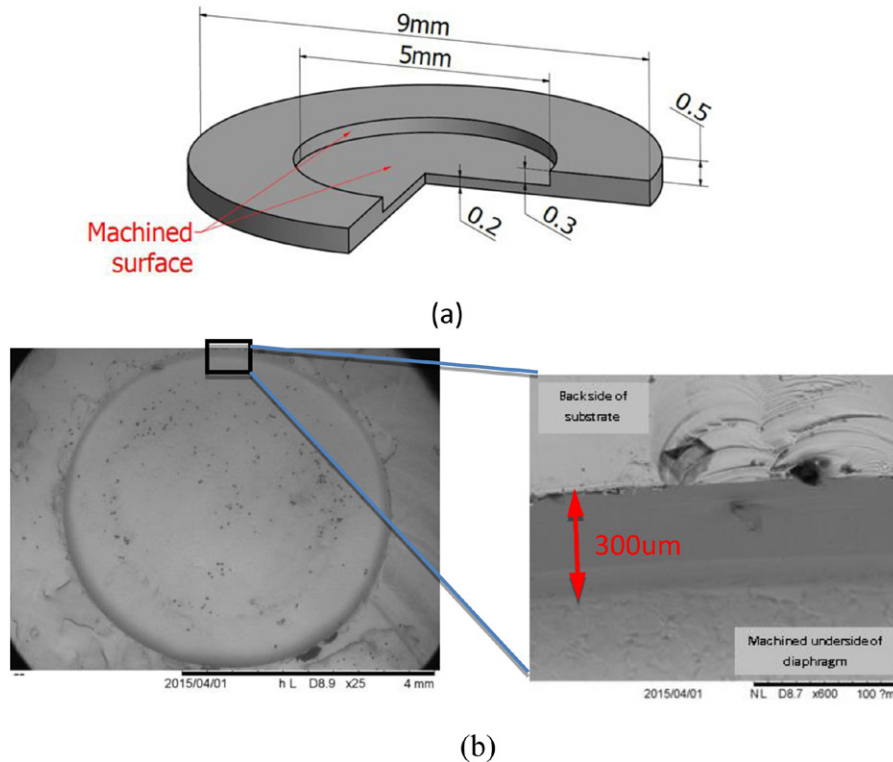
Figure 10. Prototype for biosensors (300 μm depth and 200 μm diaphragm thickness): (a) CAD model; (b) SEM images of machined LiNbO$_3$ diaphragm.

Surface roughness of the bottom surface along both the feed and cross feed direction were measured. As shown in figure 9, a clear correlation between surface roughness value and crystallographic directions existed. Those slot surfaces machined along 90° have a surface roughness (*Ra*) of around 40 nm in contrast to those slot surfaces machined along 30° or 150° on which 90 nm *Ra* was measured. Hence, micro milling should be performed either along or close to [$\bar{1}$ 0 $\bar{1}$ 0] direction with an up-milling strategy whenever possible for such materials.

5. Geometry specific fabrication and future work

Resonant based microsensors, which are commonly designed and fabricated from crystalline material to give a high quality factor resonator, offer the opportunity for high resolution measurements at low cost. However initial development costs are high due to the relatively long initial cleanroom preparation time for microfabrication approaches. In order to overcome this issue, the micro milling approach is being developed for prototyping sensors at single or small batch quantities. Piezoelectric single crystal LiNbO$_3$ is a strong material candidate as it allows for a simple sensor design whilst maintaining a high quality factor and good electronic signal recovery. To assess micro milling fabrication performance on specific geometries, polished 0.5 mm thick Z-cut LiNbO$_3$ samples were machined using 0.5 mm diameter single crystal diamond tools. Two test geometries were chosen. A circular diaphragm resonator has applications in mass sensing (Ismail 2006, Ortiz 2012) whilst ridges and channels have applications as waveguides (Hu 2007) and opto-microfluidic sensing (Bettella 2015).
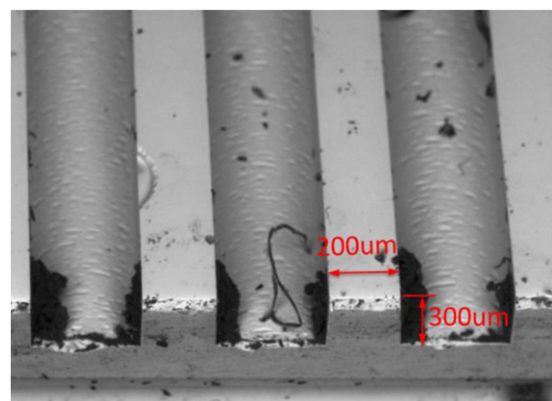
Figure 11. Micro machined channels on a single crystal LiNbO$_3$ wafer.

To produce 5 mm diameter diaphragms with 200 μm thickness for prototyping a mass biosensor, circular recesses with 5 mm diameter and depth of 300 μm were fabricated as shown in figure 10(a). Figure 10(b) shows the SEM image of a micro-machined circular diaphragm. Initial results indicate that micro milling produced a smooth vertical sidewall (surface roughness, *Ra* = 20 nm) and a moderate bottom surface finish (surface roughness, *Ra* = 80 nm). Figure 11 shows an example of machined LiNbO$_3$ waveguide/microfluidic channels. 300 μm wide by 300 μm deep channels were successfully fabricated. Very smooth vertical wall and good edge quality were obtained, though micro surface defects are still evident on the bottom surface. Performance of these devices is

being tested and future work will include investigation of post machining chemical treatments to improve the quality of the machined surface.

6. Conclusions

Micro machining of LiNbO$_3$ crystals was performed by a micro end milling process using single crystal diamond tools. Micro machined surface and edge quality, specific cutting energy, and crystallographic effect were characterised and analysed, with the aim of accomplishing machining in the ductile regime and producing a defect-free surface. The following conclusions can be drawn from this work:

- Surface morphology observation and specific cutting energy analysis revealed that ductile machining on LiNbO$_3$ can be achieved using single crystal diamond end mills at a slow feed rate and low depth of cut, and a threshold of brittle-ductile transition was obtained at a 0.3 μm/tooth under the experimental conditions in this research.
- Specific cutting energy can be used as an effective indicator to predict the ductile model cutting of brittle materials.
- Strong crystallographic orientation effect on the surface and edge quality was observed due to the high anisotropy of the material.

This research has demonstrated that diamond micro milling is a feasible process for the fabrication of LiNbO$_3$ components at a few tens to a few hundred microns scale, and shown how it can be used to translate design to prototypes at a low cost and within a short development time. Future work will be directed towards a post-machining process to remove surface defects and hybrid manufacturing. The results are also expected to be comparable with micro cutting of other brittle materials, such as germanium, silicon, silicon carbide, glass, etc.

Acknowledgments

References

Al-Shibaany Z Y A, Hedley J, Huo D and Hu Z 2014 Micromachining lithium niobate for rapid prototyping of resonant biosensors *IOP Conf. Ser.: Mater. Sci. Eng.* **65** 012030

Arif M, Rahman M and San W Y 2012 An experimental investigation into micro ball end-milling of silicon *J. Manuf. Process.* **14** 52–61

Arif M, Rahman M, San W and Doshi N 2011 An experimental approach to study the capability of end-milling for microcutting of glass *Int. J. Adv. Manuf. Technol.* **53** 1063–73

Bettella G, Pozza G, Zaltron A, Ciampolillo M V, Argiolas N, Sada C, Chauvet M and Guichardaz B 2015 Integrated opto-microfluidics platforms in lithium niobate crystals for sensing applications *Proc. SPIE 9365, Integrated Optics: Devices, Materials, and Technologies XIX* p 936517

Boyd G D, Miller R C, Nassau K, Bond W L and Savage A 1964 LiNbO$_3$: an efficient phase matchable nonlinear optical material *Appl. Phys. Lett.* **5** 234–6

Chapman R E 1984 Argon and reactive ion beam etching for SAW devices *Vacuum* **34** 417–24

Cheng K and Huo D 2013 *Micro-Cutting: Fundamentals and Applications* (Chichester: Wiley)

Cho M W, Kim D W and Cho W S 2007 Analysis of micro-machining characteristics of Si$_3$N$_4$-hBN composites *J. Eur. Ceram. Soc.* **27** 1259–65

Choong Z, Huo D, Degenaar P and O'Neil A 2015 Effect of crystallographic orientation and employment of different cutting tools on micro-end-milling of monocrystalline silicon *Proc. Inst. Mech. Eng.* B (doi: 10.1177/0954405415612379)

Darbyshire D A, Overbury A P and Pitt C W 1986 Ion and plasma assisted etching of holographic gratings *Vacuum* **36** 55–60

Davim J P 2008 *Machining: Fundamentals and Recent Advances* (London: Springer)

Foy K, Wei Z, Matsumura T and Huang Y 2009 Effect of tilt angle on cutting regime transition in glass micromilling *Int. J. Mach. Tools Manuf.* **49** 315–24

Gong H, Fang F Z, Zhang X F, Du J and Hu X T 2013 Study on the reduction strategy of machining-induced edge chipping based on finite element analysis of in-process workpiece structure *J. Manuf. Sci. Eng.* **135** 011017

Greuters J and Rizvi N H 2003 UV laser micromachining of silicon, indium phosphide and lithium niobate for telecommunications applications *OPTO Ireland* (International Society for Optics and Photonics)

Hu H, Ricken R, Sohler W and Wehrspohn R B 2007 Lithium niobate ridge waveguides fabricated by wet etching *IEEE Photon. Technol. Lett.* **19** 417–9

Huo D, Lin C, Choong Z, Pancholi K and Degenaar P 2015 Surface and subsurface characterisation in micro-milling of monocrystalline silicon *Int. J. Adv. Manuf. Technol.* **81** 1319–31

Huo D, Lin C and Dalgarno K 2014 An experimental investigation on micro machining of fine-grained graphite *Int. J. Adv. Manuf. Technol.* **72** 943–53

Ismail A K, Burdess J S, Harris A J, McNeil C J and Hedley J 2006 The principles of a MEMS circular diaphragm mass sensor *J. Micromech. Microeng.* **16** 1487–93

Johansson L, Enlund J, Johansson S, Katardjiev I, Wiklund M and Yantchev V 2012 Surface acoustic wave-induced precise particle manipulation in a trapezoidal glass microfluidic channel *J. Micromech. Microeng.* **22** 025018

Lee H J and Shin S Y 1995 Lithium niobate ridge waveguides fabricated by wet etching *Electron. Lett.* **31** 268–9

Li X, Cai M, Rahman M and Liang S 2010 Study of the upper bound of tool edge radius in nanoscale ductile mode cutting of silicon wafer *Int. J. Adv. Manuf. Technol.* **48** 993–9

Lin J, Xu Y, Fang Z, Wang M, Song J, Wang N, Qiao L, Fang W and Cheng Y 2015 Fabrication of high-Q lithium niobate microresonators using femtosecond laser micromachining for second harmonic generation *Conf. on Lasers and Electro-Optics (CLEO)*

Malshe A, Deshpande D, Stach E, Rajurkar K and Alexander D 2004 Investigation of femtosecond laser-assisted micromachining of lithium niobate *CIRP Ann. Manuf. Technol.* **53** 187–90

Ng S J, Le D T, Tucker S R and Zhang G M 1996 Control of machining induces edge chipping on glass ceramics *Proc. of the 1996 ASME Int. Mechanical Engineering Congress and Exposition, Manufacturing Engineering Division, MED(4) (Atlanta, GA, USA, November 17–22 1996)* pp 229–36

Okayama H 2003 Lithium niobate and electrooptic guided-wave optical switch *WDM Technologies* ed A K Dutta *et al* (Burlington, VT: Academic) ch 7 pp 213–84

Okuda K, Harada M, Shizuka H, Saiki T, Hamaguchi K and Utsumi Y 2014 Machining of micro groove of lithium niobate by planer-type cutting with diamond tool for fabrication of SAW device *Proc. of the 14th Euspen Int. Conf. 2014 (Dubrovnik)*

Ortiz P, Burnett R, Keegan N, Spoors J, Hedley J, Harris A, Burdess J, Raphoz N, Collet J and McNeil C 2012 Issues associated with scaling up production of a lab demonstrated MEMS mass sensor *J. Micromech. Microeng.* **22** 115032

Rusnaldy, Ko T J and Kim H S 2007 Micro-end-milling of single-crystal silicon *Int. J. Mach. Tools Manuf.* **47** 2111–9

Rusnaldy, Ko T J and Kim H S 2008 An experimental study on microcutting of silicon using a micromilling machine *Int. J. Adv. Manuf. Technol.* **39** 85–91

Shizuka H, Okuda K, Nunobiki M, Li Wand Inaoka T 2010 A study on the ductile mode cutting of lithium niobate *Adv. Mater. Res.* **126–8** 246–51

Sridhar M, Maurya D K, Friend J R and Yeo L Y 2012 Focused ion beam milling of microchannels in lithium niobate *Biomicrofluidics* **6** 012819

Takigawa R, Higurashi E, Kawanishi T and Asano T 2014 Lithium niobate ridged waveguides with smooth vertical sidewalls fabricated by an ultra-precision cutting method *Opt. Express* **22** 27733–8

Wang J J and Liao Y Y 2008 Critical depth of cut and specific cutting energy of a microscribing process for hard and brittle materials *J. Eng. Mater. Technol.* **130** 011002

Tseng W K, Lin J L, Sung W C, Chen S H and Lee G B 2006 Active micro-mixers using surface acoustic waves on Y-cut 128° $LiNbO_3$ *J. Micromech. Microeng.* **16** 539

Weis R S and Gaylord T K 1985 Lithium niobate: summary of physical properties and crystal structure *Appl. Phys.* A **37** 191–203

Winnall S and Winderbaum S 2000 Lithium niobate reactive ion etching *DTIC Document* DSTO-TN-0291 (Australia: Defence Science & Technology Organization, Department of Defence)

Wong K K 2002 *Properties of Lithium Niobate* (London: INSPEC/Institution of Electrical Engineers)

Yan J, Asami T, Harada H and Kuriyagawa T 2009 Fundamental investigation of subsurface damage in single crystalline silicon caused by diamond machining *Precis. Eng.* **33** 378–86